COUPLING TECHNIQUES FOR COMPUTATIONAL NONLINEAR TRANSIENT AEROELASTICITY

Ralf Unger, Matthias C. Haupt, Peter Horst
*Institute of Aircraft Design and Lightweight Structures
Technical University Braunschweig
Hermann-Blenk-Str. 35
38108 Braunschweig, Germany

Keywords: *Lagrange Multipliers, Aeroelasticity, Coupled Problems, Variational Methods*

Abstract

The prediction of aeroelastic effects is one of the key problems during the design process of an aircraft. One challenging aspect of this goal is to compute space and time-accurate fluid and structural interactions. In the partitioned coupling approach, well-established CFD and CSD codes are used and integrated in a flexible software environment.

One main focus of the present work is on the state and load transfer over nonconforming grids on the coupling interface. To fulfill conservation in the overall solution process, a weak formulation of the continuity conditions on the common interface based on a variational formulation of the scalar energy functional is used and Lagrange multipliers are introduced. Using Galerkin's method leads to a transfer scheme, which minimizes the L_2 error norm. An extended transfer approach, which minimizes the more general Sobolev norm will be discussed and applied to aeroelastic problems and further the use of dual-Lagrange multipliers will be presented. To solve the coupled system in a partitioned way, iterative staggered as well as simple staggered time integration schemes will be introduced.

Numerical results obtained from simulation of an oscillating one-dimensional plate in transonic flow and a three-dimensional wing example will be presented to demonstrate the applicability and performance of the concepts and to compare the properties of the different coupling techniques and transfer methods.

1 Introduction

Fluid-structure interaction gains importance for aerospace engineering applications where the target is to reach the design limits by careful analyses.

One common method for the simulation of aeroelastic effects in the time domain is to take a well-established CFD (Computational Fluid Dynamics) and CSD (Computational Structural Dynamics) code and to integrate them in a flexible software environment. This concept is assisted by increasing performance of modern computer systems.

In this partitioned solution approach, one key aspect of the overall solution process is concerned with stability and accuracy of the time integration. Another aspect in computational aeroelasticity is the transfer of loads and states between in general non-matching meshes. The use of the standard interpolation method, which is in general robust, does not fulfill the conservation law a priori.

In this paper a more general concept for treating fluid and structural coupling is employed, which is based on a variational formulation of the scalar energy functional of the full system utilizing Hamilton's principle.

This formulation leads to an interface problem which fulfills conservation of the load and state variables.

2 Variational Approach for Fluid and Structural Interaction

The use of variational principles in structural mechanics is a favorable approach to describe such continuum systems. Hamilton's principle is a more general law including additionally the dynamics of a given system, which utilizes an expression for the scalar energy as a functional, see e.g. [1].

Extensive work has been done to describe a general fluid domain by an appropriate variational principle in the past, see e.g [2]-[6]. Difficulties arise due to the dissipation term in the Navier-Stokes equation, due to the compressibility of the fluid, and due to the missing prescription of the system configuration at the final state. In the present work we forbear from deriving a lengthly calculation but we state that a Hamilton's formalism exists for a single fluid domain including viscous effects and compressibility.

Assuming a given functional principles for a single fluid and solid, the variational functional of the whole coupled system can be divided into an interior functional and a connectivity potential [7]:

$$\Pi = \sum_n (\Pi_n(\phi^{(n)}) - \Pi_{cn}), \quad n = s, f, \qquad (1)$$

where ϕ contains all state variables of the system, Π_n is the scalar energy functional of one subsystem, and Π_{cn} denotes the connectivity potential to a connectivity frame (three-field approach) using localized Lagrange multipliers as in [7], [8]. Forgoing the use of an intermediate connectivity frame (two-field approach), the functional leads to:

$$\Pi = \sum_n \Pi_n(\phi^{(n)}) - \Pi_{fs}, \quad n = s, f, \qquad (2)$$

with the connectivity potential being:

$$\Pi_{sf} = \int_{\Gamma_{sf}} \lambda_i^{(sf)} \left(\phi_i^{(s)} - \phi_i^{(f)} \right) \mathrm{d}\Gamma_{sf}. \qquad (3)$$

The state vector ϕ_i is set to the displacements u_i and thus the energy of the interface in terms of Hamilton's principle could be written as (neglecting viscous stresses):

$$E_{sf} = \int_{t_1}^{t_2} \left[\int_{\Gamma_{sf}} \left(u^{(f)} p^{(f)} - u^{(s)} p^{(s)} \right) \mathrm{d}\Gamma_{sf} \right] \mathrm{d}t, \qquad (4)$$

where p denotes the pressure. Therefore, it can be claimed that the energy in a coupled system due to a partitioned analysis neither increases nor decreases. Furthermore, the physical meaning of the Lagrange multipliers should be clear.

Using elementwise interpolations of the structural state variables (usually finite element methods) and of the fluid unknowns (e.g. finite volume method) as well as for the Lagrange multipliers, the variation $\delta\Pi = \sum_n \delta\Pi_n(\phi^{(n)}) - \delta\Pi_{fs} = 0$ leads to a set of discretized equations:

$$\boldsymbol{M}^{(s)}\ddot{\boldsymbol{u}}^{(s)} + \boldsymbol{F}_i^{(s)} - \boldsymbol{F}_e^{(s)} + \boldsymbol{M}_{\lambda u}^{(s)}\boldsymbol{\lambda}^{(sf)} = \boldsymbol{0} \qquad (5)$$

$$\boldsymbol{M}^{(f)}\dot{\boldsymbol{W}}^{(f)} + \boldsymbol{R}^{(f)}(\boldsymbol{W}^{(f)}) = \boldsymbol{0} \qquad (6)$$

$$\boldsymbol{M}_{\lambda u}^{(s)\,T}\boldsymbol{u}^{(s)} - \boldsymbol{M}_{\lambda u}^{(f)\,T}\boldsymbol{u}^{(f)} = \boldsymbol{0} \qquad (7)$$

Eqn. (5) represents the structural subsystem, where $\boldsymbol{M}^{(s)}$ denotes the mass matrix of the structural system and $\boldsymbol{F}_e^{(s)}$ and $\boldsymbol{F}_i^{(s)}$ are the vector of prescribed and internal forces, respectively. The last term, $\boldsymbol{M}_{\lambda u}^{(s)}\boldsymbol{\lambda}^{(sf)}$, arises due to the use of Lagrange multipliers and acts as a physical flux (traction) on the structure. Eqn. (6) stands for the fluid subsystem and the conservative flow variables $W_i^{(f)} = [\rho^{(f)}, \rho^{(f)}U_1^{(f)}, \rho^{(f)}U_2^{(f)}, \rho^{(f)}U_3^{(f)}, \rho^{(f)}E^{(f)}]^T$ at each fluid (grid) point depends on the interface displacements $u^{(f)}$. Therefore, the fluid subsystem can be treated as a continuous system, in which a traction field (pressure and viscous stress) acts on an interface and thus the interface distorts, see also [8]. Hence, the vector $\boldsymbol{W}^{(f)}$ contains implicitly the term $\boldsymbol{M}_{\lambda u}^{(f)}\boldsymbol{\lambda}^{(sf)}$. The vector $\boldsymbol{R}^{(f)}$ stands for the complete spatial discretization or residual. The interface problem of the coupled system is expressed with Eqn. (7) and the coupling

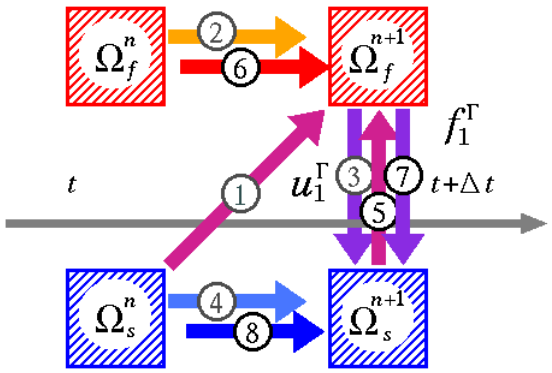

Figure 1: Time integration scheme for the coupled system

matrices hold:

$$\boldsymbol{M}_{\lambda u}^{(i)} = \int_{\Gamma_{sf}} \boldsymbol{N}_u^{(i)} \boldsymbol{N}_\lambda^T \, \mathrm{d}\Gamma_{sf} \quad \text{for} \quad i = s, f. \quad (8)$$

This approach is common in fluid and structural interaction problems, and the unknowns are reduced to the field variables, the interface state variables and one discrete Lagrange multiplier. The whole system of equations consisting of (5), (6) and (7) can be solved by an iterative process for every time step, see [9].

3 Time Integration and Equilibrium Iteration

Due to the use of separate analysis codes for the fluid and structural subsystem, an iterative scheme must be used. The classical approach achieving equilibrium in the two subsystems and in every time-step is the Dirichlet-Neumann iteration, utilizing a relaxation between an outdated and an updated state:

$$\boldsymbol{u}_{k+1}^{(s)} = \omega \hat{\boldsymbol{u}}_{k+1}^{(s)} + (1-\omega)\boldsymbol{u}_k^{(s)} \quad \text{on } \Gamma_{sf}, \quad (9)$$

where $\hat{\boldsymbol{u}}_{k+1}^{(s)}$ results from a Dirichlet-Neumann step and ω denotes the relaxation parameter, which is frequently set to 0.75-0.85. In the above equation a subscript denoting the time step is omitted. An automatic evaluation of ω during each iteration can be performed through an extension of the gradient method.

With this equilibrium iteration, the time integration can be done in the following way, see Fig. 1; step 1 predicts the interface state of the structure representation and transfers it to the fluid, followed by the fluid analysis for $t+\Delta t$ including a grid deformation mechanism in step 2, and the load transfer in step 3 before the structural analysis for $t+\Delta t$ in step 4. Appending a k-multiple sequence of step 5 to 8 with relaxation, the equilibrium state of the interface can be achieved and the overall order of time accuracy is according to the minimal one reached in the subsystems. Performing only step 1 to 4 ($k = 0$) with $\omega = 1$ results in the so-called loose coupling or simple staggered approach. Regardless of the time accuracy implemented in the analysis codes of the subsystems, this scheme is usually first order time accurate, due to the incomplete fulfillment of the continuity conditions. The scheme can be improved by an appropriate predictor $\tilde{\boldsymbol{u}}_{n+1}^{(s)}$ in step 1 and one natural choice is, [10]:

$$\tilde{\boldsymbol{u}}_{n+1}^{(s)} = \boldsymbol{u}_n^{(s)} + \Delta t \dot{\boldsymbol{u}}_n^{(s)} + \tfrac{\Delta t^2}{2} \ddot{\boldsymbol{u}}_n^{(s)} \quad \text{on } \Gamma_{sf}. \quad (10)$$

4 Transfer of Loads and Displacements

As seen in the section above, a weak formulation of the state transfer, Eqn. (7), arises due to the variation of the scalar energy functional of the system. The Lagrange multipliers are discretized along the interface independent of the interpolation of the state variables on the interface surface. One basic limitation of the discretization of the multipliers lies in choosing the number of degrees of freedom of the multipliers, which may not exceed the number of degrees of freedom of any state variable on the interface, since otherwise the system would be overestimated [11].

The freedom of choice opens a broad range of possibilities for the multipliers using with separate algorithms for each subdomain, which are discretized in a separate way.

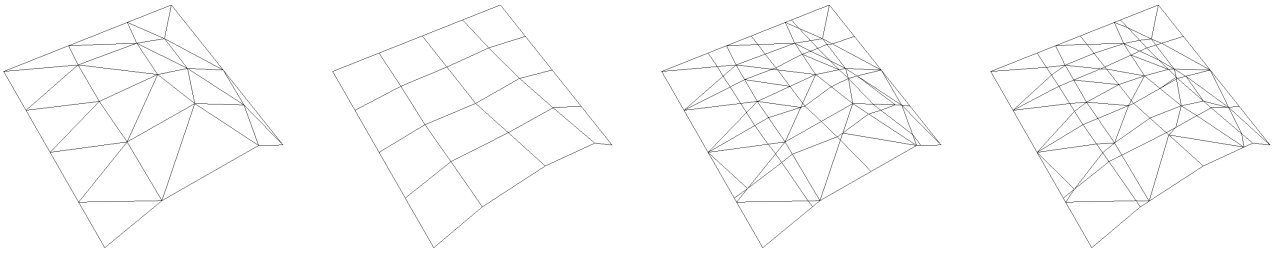

(a) fluid mesh (b) structural mesh (c) merged mesh with fluid reference (d) merged mesh with structural reference

Figure 2: Construction of a merged mesh

4.1 Load Transfer

The load transfer should be constructed transposed to the transfer of the interface states to ensure the equilibrium of energy at every time step. The variation process of the scalar energy at the interface given in Eqn. (4) yields after discretization:

$$\delta \boldsymbol{u}^{(s)\,T} \boldsymbol{f}^{(s)} = \delta \boldsymbol{u}^{(f)\,T} \boldsymbol{f}^{(f)} \quad \text{on } \Gamma_{sf}, \tag{11}$$

where $\boldsymbol{f}^{(i)}$ denotes the discrete nodal forces at the interface surface. Given for instance a coupled system with the state transfer according to eqn. (7), the transposed load transfer yields:

$$\boldsymbol{f}^{(s)} = \boldsymbol{M}^{(s)}_{\lambda u} [\boldsymbol{M}^{(f)}_{\lambda u}]^{-1} \boldsymbol{f}^{(f)}. \tag{12}$$

4.2 State Transfer Schemes

In the following section some popular transfer schemes are introduced, which are often used in fluid-structure interaction problems. Most of the schemes differ only in the choice and on the location of the Lagrange multipliers.

4.2.1 Conservative Interpolation

Taking Dirac delta function on the fluid interface representation for the Lagrange multipliers, the integral vanishes and the scheme reduces to the evaluation of the structural shape functions at the fluid nodes. This transfer procedure is similar to that presented in [12] and is often referred to as conservative interpolation or node projection scheme, since the fluid nodes on the interface are mapped to the closest structural interface element.

4.2.2 Quadrature-based Integration

Unfortunately, the conservative interpolation could lead to unphysical effects and an improvement is the use of the fluid shape functions for the Lagrange multipliers $\boldsymbol{N}_\lambda = \boldsymbol{N}^{(f)}_u$ (Galerkin's method). This choice is advantageous, since the matrix $\boldsymbol{M}^{(f)}_{\lambda u}$ is positive definite and thus regular. The transposed load transfer according to eqn. (12) and neglecting viscous stresses is evaluated by:

$$\boldsymbol{f}^{(s)} = \bar{\boldsymbol{M}}^{(sf)} [\bar{\boldsymbol{M}}^{(ff)}]^{-1} \boldsymbol{f}^{(f)} = \bar{\boldsymbol{M}}^{(sf)} \boldsymbol{p}^{(f)}. \tag{13}$$

This scheme is equivalent to the scheme proposed in [13] and also minimize the L_2-norm of the jump of the pressure field across the interface. The main difficulties lies in the computation of the matrix $\bar{\boldsymbol{M}}^{(sf)}$, which can be done by the aid of quadrature points and therefore this scheme is frequently referred to as quadrature-projection scheme. The numerical integration can be done on the fluid or on the structural representation of the interface. Accuracy could be lost due to the violation of regularity, which is assumed by the quadrature rule and due to fact that some elements do not receive any quadrature points depending on the mesh size of the fluid and structural mesh. This problem can be solved by introducing more quadrature points or by an adaptive mesh refinement.

In Fig. 3, a sequence of refinement levels of the integration mesh of a simple three-dimensional configuration is shown, where the integration mesh is based on the structural

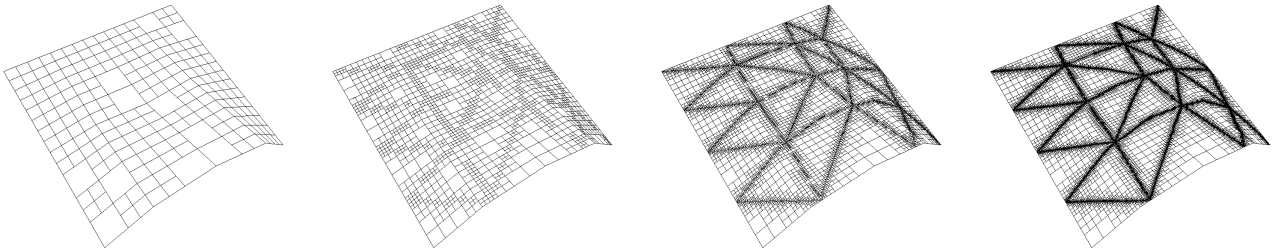

(a) Level 2 (b) Level 4 (c) Level 6 (d) Level 8

Figure 3: Adaptive quadtree-based refinement of the integration mesh

mesh depicted in Fig. 2b and the fluid mesh is shown in Fig. 2a. The adaptive mesh refinement is based on a hierarchical quadtree data structure of the mesh and is a simple and robust method to increase the accuracy for arbitrary meshes.

Another possibility to increase the accuracy of a transfer scheme is the utilization of an integration mesh which is appropriately constructed from the fluid and structural representation of the interface, Fig. 2. From Fig. 2c and 2d it can be seen that two possibilities of such merged mesh exist in a three-dimensional space. Both have the same combinational structure but different geometric realization. Using such an integration mesh, the regularity assumption of the quadrature rule remains valid and the main task of the integration procedure turns to the automatic build-up of such mesh (which is a non-trivial problem in 3d) and to the robust projection of quadrature points to the other representations of the interface.

While both methods, adaptive mesh refinement and merged mesh, increase the accuracy considerably, the former one is more general and can be used for almost every configuration. The definition of a merge mesh depends noticeably on the used meshes.

4.2.3 Dual-Lagrange Multiplier

In the above scheme the matrix $\boldsymbol{M}_{\lambda u}^{(f)}$ from Eqn. 7) has to be inverted to get $\boldsymbol{u}^{(f)}$. Although the matrix is sparse and positive definite, this inversion process is often the bottle neck of the transfer schemes in systems with many degree of freedoms. By choosing an appropriate space for the Lagrange multipliers depending on the shape functions of the fluid interface representation this matrix can be diagonalized. This is the idea of the so-called dual-Lagrange multipliers introduced by Wohlmuth in [14, 15]. Consider for instance an one-dimensional problem with fluid elementwise shape functions on the interface being $\tilde{\boldsymbol{N}}_u^{(f)\,T} = [1-\xi, \xi]$, the appropriate dual-Lagrange multipliers for an element yields $\tilde{\boldsymbol{N}}_\lambda^T = [-3\xi + 2, 3\xi - 1]$. Corresponding dual-Lagrange multipliers can be found for two-dimensional elements and with higher orders.

4.2.4 Minimizing the Sobolev-norm

The use of Galerkin's method to construct a transfer scheme minimizes the L_2 norm of the jump of the displacements across the interface, which is equivalent to the Sobolev-norm H^0. In [16] a transfer scheme was proposed, which minimizes the Sobolev-norm H^1:

$$\frac{\partial\left(\int_{\Gamma_{sf}} \sum_{n=0}^{1} \left|\alpha_n D^n (u^{(f)} - u^{(s)})\right|^2 \mathrm{d}\Gamma_{sf}\right)^{\frac{1}{2}}}{\partial \hat{u}_i^{(f)}} = 0 \quad (14)$$

where $\hat{u}_i^{(f)}$ are the discrete nodal values of the fluid displacements and D^n operates to a function to get the nth derivatives in space. After the discretization process the minimization leads to:

$$\left(\bar{\boldsymbol{M}}^{(ff)\,T} + \alpha \bar{\boldsymbol{K}}^{(ff)\,T}\right) \boldsymbol{u}^{(f)} = \left(\bar{\boldsymbol{M}}^{(sf)\,T} + \alpha \bar{\boldsymbol{K}}^{(sf)\,T}\right) \boldsymbol{u}^{(s)}, \quad (15)$$

with $\bar{\boldsymbol{K}}^{(ij)}$ being the stiffness matrices evaluated in the same way as above. The transposed scheme (transfer of tractions) is also conservative and for integration, the methods described above (adaptive mesh refinement, merged meshes), may be used here too.

5 Application to Aeroelasticity

In the following, some examples will be given to illustrate the applicability of the presented concepts. The first application is the panel flutter problem; i.e. a simply supported panel over which a compressible inviscid fluid flows. The panel is modeled using the nonlinear von Karman-plate theory with constant plate behavior in spanwise direction [17]. Under defined conditions the panel exhibits the flutter phenomena.

As a three-dimensional application the well-published AGARD wing 445.6 is presented. If accurately simulated, this wing shows a damped oscillation, otherwise flutter with increasing amplitude can be observed

Furthermore, the fluid flow solver uses a finite volume scheme and solves the Euler equation. For a description of the fluid flow solver see [18]. The time integration within the fluid solver is done by an implicit dual-time stepping approach. A deformation module transfers a surface grid deformation to a fluid flow domain. The geometric conservation law is considered within the solver module.

5.1 Panel Flutter Problems

For an one-dimensional Karman-plate (constant plate behavior in spanwise direction) the structural functional can be written as:

$$\Pi_s(w) = \int_{t_1}^{t_2} \Bigg[\int_0^l \frac{1}{2} \Bigg(D\theta_{,x}^2 + \kappa G h (w_{,x} - \theta)^2 + \frac{N_0 + N_x}{2} w_{,x}^2 \Bigg) \mathrm{d}x - \int_0^l \frac{1}{2} \left(\rho_s h w_{,t}^2 + \frac{\rho_s h^3}{12} \theta_{,t}^2 \right) \mathrm{d}x - \int_0^l w \bar{p} \, \mathrm{d}x \Bigg] \mathrm{d}t, \tag{16}$$

where $\theta = w_{,x}$ is the rotation of the plate section, D and G are the plate stiffness and shear module, respectively. The nonlinearities occur due to N_x, which depends on $w_{,x}$.

In the present contribution the fluid interface consists of 445 nodes while the structural discretization may have 10, 20, 50 or 100 elements. The parameters for the fluid flow were: $Ma_\infty = 1$, $p_\infty^{(f)} = 75867\,\mathrm{N/m^2}$, $\rho_\infty^{(f)} = 1.225\,\mathrm{kg/m^3}$, i.e. transonic flutter case. The structural parameters were set to: $\rho^{(s)} = 2700\,\mathrm{kg/m^3}$, Young's module $E = 7.1 \cdot 10^{10}\,\mathrm{N/m^2}$, panel thickness $h = 0.004537\,\mathrm{m}$. The nonlinear structural equations are solved utilizing a Newton-Raphson iteration and time integration is performed using a Newmark scheme. The panel is initially perturbed by an overpressure on the underneath of the panel.

5.1.1 Influence of Transfer Schemes

Fig. 4a shows the comparison of the midpoint deflection of the panel over the time using the quadrature-based transfer scheme, whereby the integration is performed on the fine fluid mesh using an overall time step of $\Delta t = 0.0005\,\mathrm{s}$ and an iterative staggered procedure. As one can observe even for a very coarse mesh for the structure a flutter behavior of the panel is obtained. These results fit very well with results published in [17]. The main difference using a coarser structural mesh lies in the obtained flutter frequency which decrease with coarser meshes.

Contrary to the quadrature-based transfer, one could observe that the standard interpolation, which is quite often used in fluid-structure interaction fails already with using 50 structure elements for the panel, Fig. 4b. The solution obtained with 100 elements is obtained as above, using the quadrature-based transfer. With 50 structural elements the solution losts its stability after some cycles and no flutter could be seen, if 20 structural elements were used. This is due to the properties that such schemes do not guarantee a conservative transfer and that sharp gradients (shocks) are

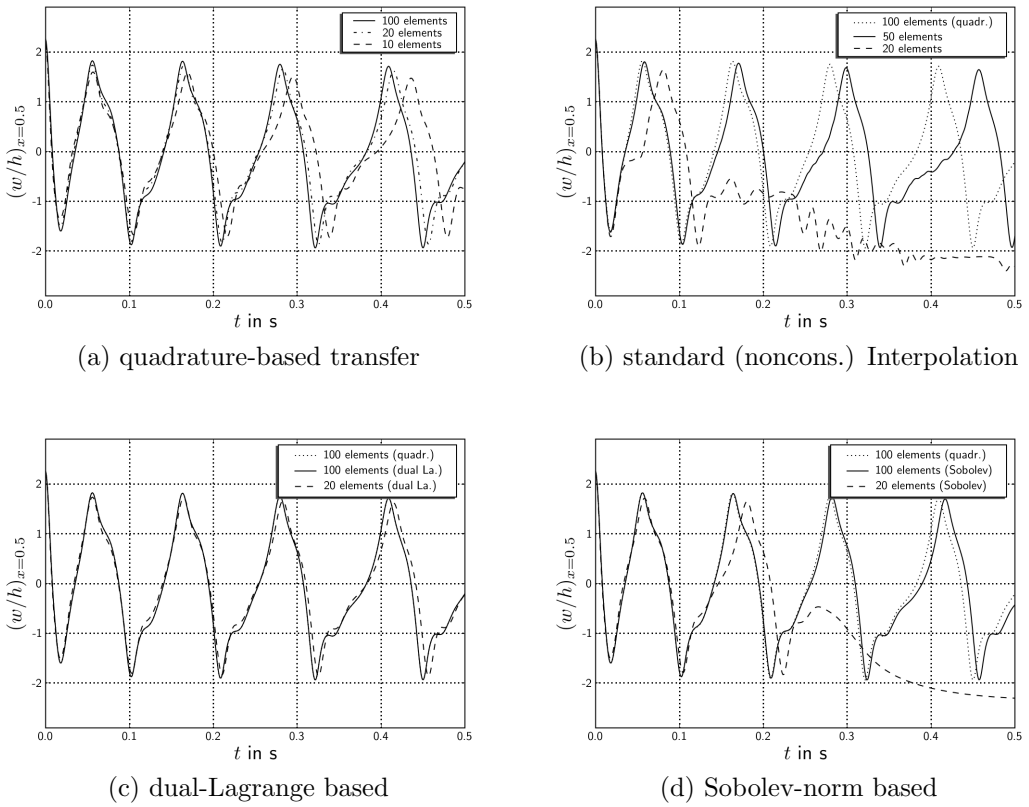

(a) quadrature-based transfer

(b) standard (noncons.) Interpolation

(c) dual-Lagrange based

(d) Sobolev-norm based

Figure 4: Time history of the panel midpoint deflection using different transfer schemes

not captured accurately.

The time history of the midpoint deflection using dual-Lagrange multipliers shows exactly the same behavior as for the quadrature-based transfer scheme, Fig. 4c, i.e. both curves labeled with 100 element show no difference. The advantage of the dual-Lagrange multipliers lies in the computational costs inverting the matrix $\boldsymbol{M}_{\lambda u}^{(f)}$. Therefore this technique is favorable for transfer schemes.

In Fig. 4d the midpoint deflection of the panel is shown using the Sobolev-norm based transfer scheme, whereby the integration is performed on a merged mesh. For 100 structural elements almost the same time history as for the transfer using the quadrature points or dual-Lagrange multiplier could be identified and for 20 structural elements no flutter of the panel occurs. For α, a value of $\alpha = 0.3$ is used. To express more general statements using Sobolev based transfer more parameter studies need to be performed.

5.1.2 Influence of the Time-Integration Scheme

In the following, some detailed comments on the influence of the overall time-integration procedure are given. In Fig. 5 the midpoint deflection of the panel using iterative and simple (with and without predictor) staggered schemes is depicted. The present calculations were run with the dual-Lagrangian based state and load transfer with the fluid mesh being the same as described above and a structural discretization of 100 elements. As mentioned in the section earlier, the studied panel flutter case is on the stability border as published in [17]. Therefore, the first chosen time step was set to $\Delta t = 0.0001\,\mathrm{s}$, Fig. 5a, and the results obtained by the simple staggered scheme without a predictor remain fairly enough. Utilizing the second order predictor of Eqn. (10) the simple staggered time-integration method shows no difference to the iterative staggered

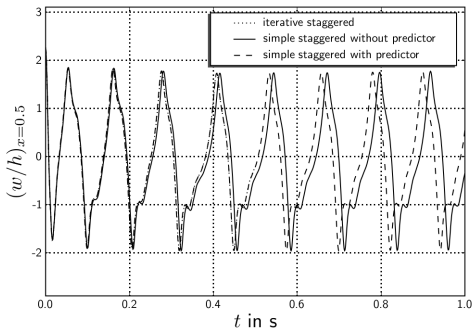

(a) Time Step: $\Delta t = 0.0001\,\mathrm{s}$

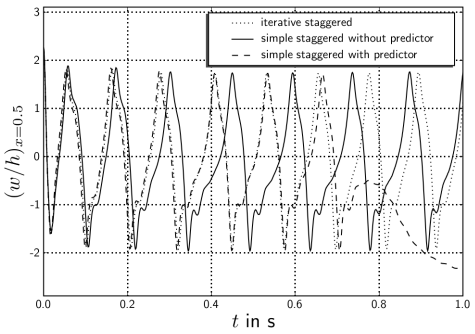

(b) Time Step: $\Delta t = 0.0005\,\mathrm{s}$

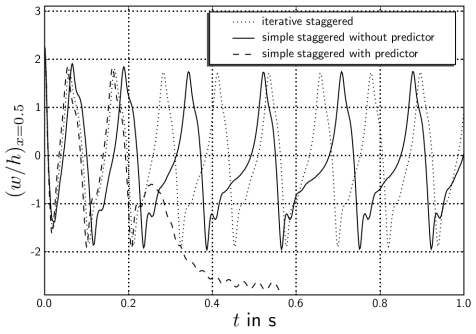

(c) Time Step: $\Delta t = 0.001\,\mathrm{s}$

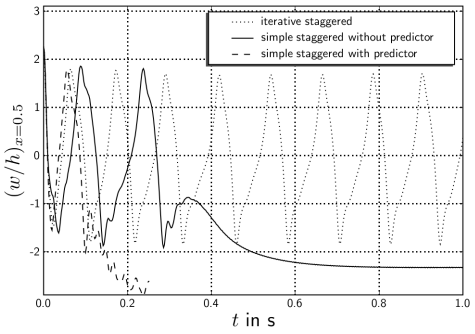

(d) Time Step: $\Delta t = 0.002\,\mathrm{s}$

Figure 5: Time history of the panel midpoint deflection using different time-integration schemes

scheme.

Changing the time step size to $\Delta t = 0.0005\,\mathrm{s}$, Fig. 5b, the predicted flutter frequency of the simple staggered approach without predictor differs noticeably from that one obtained by the iterative method. Using a second order predictor, the time history of the midpoint deflection is closer to the curve of the iterative staggered schemes but becomes unstable after some cycles, contrary to the staggered method without predictor.

Using a time step of $\Delta t = 0.001\,\mathrm{s}$, Fig. 5c, the same statements can be given and the loss of stability utilizing a predictor appears earlier. Increase the time step size further, the staggered scheme without predictor will not show the panel flutter phenomenon, Fig. 5d.

5.2 Flutter Analysis of the AGARD Wing 445.6

To demonstrate the applicability of the presented schemes to three-dimeinsional problems, the flutter analysis of the AGARD wing 445.6, see [19], is considered. The wing has a 45 deg quarter-chord sweep angle, a panel aspect ratio of 1.65, a taper ratio of 0.66 and consists of a NACA 65A004 airfoil section.

The analysis of this wing is widely published in literature and here the 2.5 ft weak-

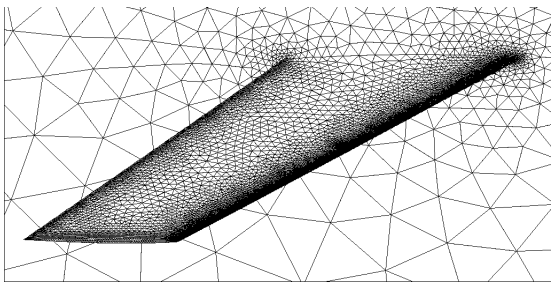

Figure 6: Fluid mesh of the AGARD wing 445.6

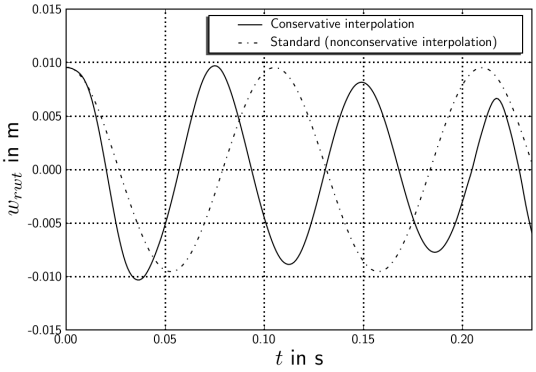

Figure 7: Time history of the rear wing tip deflection using conservative and standard interpolation

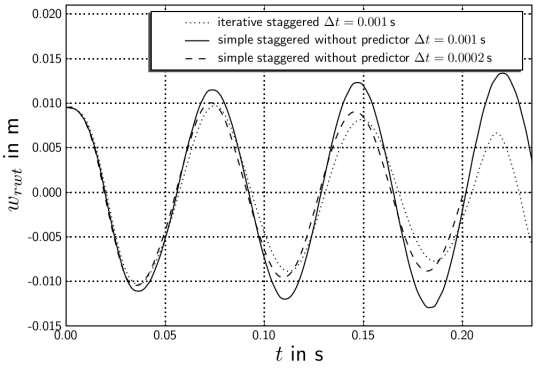

Figure 8: Time history of the rear wing tip deflection using different time integration schemes

end model number 3 is used. A part of the fluid mesh is shown in Fig. 6 and the structure is modeled using 20x20 shell elements. The structural properties were designed to the first five eigenfrequencies of the wing, see [19] and the first eigenmode is a bending mode with 9.83 Hz. The fluid mesh consists of 334861 tetrahedrals and 64943 nodes and the fluid interface holds 30666 elements and 15380 nodes.

Like the panel flutter problem, the fluid flow is computed using a finite volume scheme solving the Euler equation and advancing forward in time is done by an implicit dual-time stepping scheme. The structural equations are solved by a commercial finite element code using linear shell theory and the Newmark time integration scheme. The freestream conditions of the fluid flow are chosen to be: $Ma_\infty = 0.901$, $p_\infty^{(f)} = 5745,67\,\mathrm{N/m^2}$, and $\rho_\infty^{(f)} = 0.099477\,\mathrm{kg/m^3}$. The structural parameters are set to: $\rho^{(s)} = 421\,\mathrm{kg/m^3}$, $E_1 = 3.5455 \cdot 10^9\,\mathrm{N/m^2}$, $E_2 = 4.162 \cdot 10^8\,\mathrm{N/m^2}$, $G = 4.119 \cdot 10^8\,\mathrm{N/m^2}$. The thickness of the shell elements are modeled using the NACA 65A004 airfoil profile. The calculations were run with an overall time step of $\Delta t = 0.001\,\mathrm{s}$ and the wing was perturbed initially with the first bending mode.

In Fig. 7 the time history of the deflection of the rear wing tip is depicted and both calculations were run with an iterative time integration scheme. The transfer scheme of the first calculation is the conservative interpolation, which is sufficient enough due to the fine fluid mesh. This behavior of the wing fits very well with computations published in [20]. The use of the quadrature based transfer scheme or the utilization of the dual-Lagrangian's should hold principally the same history due to the fine fluid mesh compared to the structural mesh. Conservative interpolation was chosen here because of its robustness and efficiency. The second calculation uses the nonconservative standard interpolation and as one can observe the difference between both plots is not negligible. A snapshot of the deflected wing at the time $t = 0.075\,\mathrm{s}$ is shown in Fig. 9.

The influence of the time-integration scheme is depicted in Fig 8 using the conservative interpolation for the load and state transfer. The curve representing the iterative staggered procedure shows a damped oscillation of the initially perturbed wing while the wing simulated with the aid of a simple staggered method shows an increasing amplitude of the wing flutter when using a time step of $\Delta t = 0.001\,\mathrm{s}$. Choosing a smaller time step of $\Delta t = 0.0002\,\mathrm{s}$ leads to a similar behavior as for the iterative scheme but the computational costs are almost identical. This results also fits very well with those published in [20].

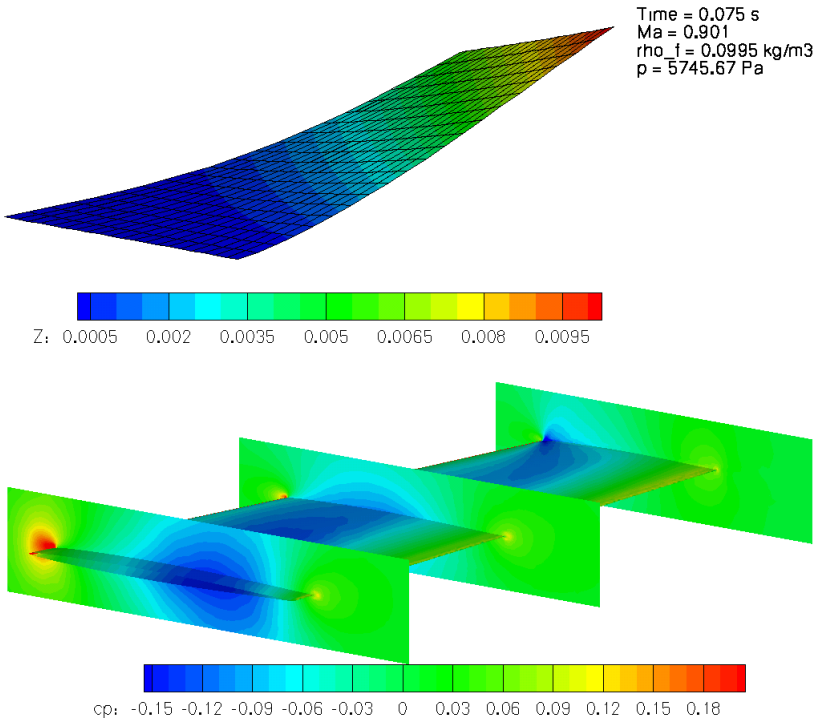

Figure 9: Pressure field and structural deflection of the AGARD wing at $t = 0.075\,\mathrm{s}$

6 SUMMARY AND CONCLUSION

In the present paper a variational formulation based on Hamilton's principle is adopted for fluid and structural coupled problems. Using the two-field approach the interface problem occurs as a weak formulation of the interface condition. Different transfer schemes were employed, which share the property of load conservation across the interface of non-matching meshes. For the time-integration of the overall system, iterative and simple staggered procedure were employed. Applied to the panel flutter problem, different behavior of the results could be observed depending on which transfer and time-integration method was used. The use of dual-Lagrangians is promissing since the computational costs are less than for the generic quadrature based transfer scheme, while the results are identical. Utilizing the concept of dual-Lagrangians for three-dimensional applications is still demanding and one has to find appropriate shape functions. Furthermore, the importance of a conservative load transfer could be shown for the panel flutter problem as well as for the three-dimensional wing example. Simple staggered procedures with a second order predictor tend to be unstable while those schemes without a predictor compute different panel flutter frequencies. Thus, it could be shown here, that for a precise prediction of the panel flutter problem an accurate transfer as well as a proper time integration scheme need to be used.

For the three-dimensional wing structure, an undamped oscillation is obtained while for the iterative staggered scheme a flutter with decreasing amplitude appears.

References

[1] J.N. Reddy, *Energy Principles and Variational Methods in Applied Mechanics*. John Wiley & Sons, New Jersey, 2002.

[2] H. Benaroya and T. Wei, Hamilton's Principle for Viscous External Fluid-Structure Interaction. *Journal of Sound and Vibration*, **238**(1), 113–145, 2000.

[3] T. Tran-Cong, A variational principle for fluid mechanics. *Archive of Applied Mechanics*, **67**, 96–104, 1996.

[4] R.R. Kerswell, Variational Principle for the Navier-Stokes equation. *Physical Review E*, **59**(5), 5482–5494, 1999.

[5] R.J. Becker, Lagrangian/Hamiltonian Formalism for Description of Navier-Stokes Fluids. *Physical Review Letters*, **58**(14), 1419–1422, 1987.

[6] E. Kock and L. Olson, Fluid-Structure Interaction Analysis by the Finite Element Method – A variational Approach. *Int. J. Numer. Meth. Engng.*, **31**, 463–491, 1991.

[7] K.C. Park and C.A. Felippa, A Variational Principle for the Formulations of Partitioned Structural Systems. *Int. J. Numer. Meth. Engng.*, **47**, 395–418, 2000.

[8] K.C. Park, C.A. Felippa and R. Ohayon, Partitioned formulation of internal fluid-structure interaction problems by localized Lagrange multipliers. *Comput. Methods Appl. Mech. Engrg*, **190**, 2989–3007, 2001.

[9] M.C. Haupt and P. Horst, Coupling of fluid and structure analysis codes for air and spacecraft applications. *Proc. of First MIT Conference on Computational Solid and Fluid Mechanics in: Computational Solid and Fluid Mechanics*, 2, 1226–1231, 2001.

[10] S. Piperno, C. Farhat and B. Larrouturou, Partitioned procedures for the transient solution of coupled aeroelastic problems Part I: Model problem, theory and two-dimensional application. *Comput. Methods Appl. Mech. Engrg*, **124**, 79–112, 1995.

[11] J.B. Ransom, Interface Technology for Geometrically Nonlinear Analysis of Multiple Connected Subdomains. *AIAA-Paper 97-1298*, 1997.

[12] C. Farhat, M. Lesoinne and P. LeTallec, Load and motion transfer algorithms for fluid/structure interaction problems with non-matching discrete interfaces: Momentum and energy conservation, optimal discretization and application to aeroelasticity. *Comput. Methods Appl. Mech. Engrg*, **157**, 95–114, 1998.

[13] J.R. Cebral and R. Löhner, Conservative Load Projection and Tracking for Fluid-Structure Problems. *AIAA-Journal*, **35**(4), 687–692, 1997.

[14] B.I. Wohlmuth, A mortar finite element method using dual spaces for the Lagrange multiplier. *SIAM Journal on Numerical Analysis*, **38**, 989–1012, 2000.

[15] M.A. Puso, A 3D mortar method for solid mechanics. *Int. J. Numer. Meth. Engng.*, **59**, 315–336, 2004.

[16] X. Jiao and M.T. Heath, Common-refinement based data transfer between non-matching meshes in multiphysics simulations. *Int. J. Numer. Meth. Engng.*, **61**, 2402–2427, 2004.

[17] R. Massjung, Numerical Schemes and Well-Posedness in Nonlinear Aeroelasticity. *PhD-Thesis*, RWTH Aachen, Faculty of Mathematics, Computer Science and Natural Sciences, 2000.

[18] T. Gerhold, M. Galle, O. Friedrich and J. Evans, Calculations of Complex Three-Dimensional Configurations Employing the DLR-TAU-Code. *AIAA-Paper 97-0167*, 1997.

[19] E.C. Yates, AGARD standard aeroelastic configurations for dynamic response, candidate configuration I - Wing 445.6. *NASA TM-100492*, 1987.

[20] C. Farhat and M. Lesoinne, Two efficient staggered algorithms for the serial and parallel solution of three-dimensional nonlinear transient aeroelastic problems. *Comput. Methods Appl. Mech. Engrg*, **182**, 499–515, 2000.